Supplementary information for
"Triple-phase ceramic 2D nanocomposite with enhanced thermoelectric properties"

Michael Bittner[1], Nikola Kanas[2], Richard Hinterding[1], Frank Steinbach[1], Dennis Groeneveld[1], Piotr Wemhoff[1], Kjell Wiik[2], Mari-Ann Einarsrud[2], Armin Feldhoff[1]

[1]Institute of Physical Chemistry and Electrochemistry,
Leibniz University Hannover, Germany

[2]Department of Materials Science and Engineering,
Norwegian University of Science and Technology, Norway

1 Supplementary

Schemes, diagrams both SEM and TEM micrographs were created using OriginPro 9.1G, ImageJ, Diamond and Digital Micrograph. Figures were arranged, merged and saved using PowerPoint 2010 and Photoshop CS5. Table S 1 shows the ionic radii of the substituted elements and inserted dopants. According to the similarity of the ionic radii of the elements used, doping should be possible. The XRD patterns of the Na_xCoO_2 (NCO) and $Bi_2Ca_2Co_2O_9$ (BCCO) phases, shown in Figure S 1 refer to Figure 2 in the main text. A step size of 0.003942, a time per step of 1.1 seconds, a voltage of 40 kV and a current of 40 mA were used in the XRD experiments. Pure NCO and nearly pure BCCO phases were subjected to SEM and elemental distribution analyses of polished cross-sections, as shown in Figure S 2a-d. Vibration-polished cross-section specimens were prepared by a multistep (30 μm, 15 μm, 6 μm, 3 μm and 1 μm diamond lapping films) polishing program using a Techprep from Allied - High Tech Products, Inc., followed by vibration polishing using a Buehler Vibromet-2 and a 50 nm colloidal alumina suspension. TEM specimens were prepared similar to SEM specimens and put on a TEM grid. The specimens were pinched out using a precision ion polishing system (Ar-ion) Model 691 from Gatan. The BCCO phase decomposes at approximately 1023 K, and Ca-containing phases are formed; see Figure S 1[1]. Figure S 3 gives detailed elemental distribution information referring to Figure 4a-c in the main document. The interdiffusion of Ca into the NCO phase is clearer, and the very thin layers of NCO and BCCO are clearly visible in the Na, Ca and Bi signals shown in Figures S 3d-f and 4a-d. The insets of Figure 4d-f in the main document are enlarged for a better readability in Figure S 5a-f. Additional TEM micrographs of other sites of the CCO-30-35-10 nanocomposite ceramic are shown in Figures S 6, 7 and 8. These other sites clarify the composition and thickness of different layers within the material. These sequences continue throughout the ceramic. Comparing Figure S 6 and Figure S 7 shows that the amount of interdiffusion of Ca into the NCO phase is not constant, suggesting that the degree of interdiffusion might also depends on thickness and surroundings (e.g., being embedded between BCCO phases). Figure S 9 illustrates the measured heat capacities C_P of CCO and nanocomposite ceramics as a function of temperature in the range from 313 K to 1173 K. The C_P values reached approximately 0.83 J $\cdot$ g^{-1} $\cdot$ K^{-1} at 1073 K for a CCO-30-35-10 nanocomposite ceramic. The nanocomposite ceramics showed only small differences in C_P from those of undoped CCO. The system was calibrated and the sapphire method was used. The sensitivity S and heat capacity C_P were calculated as described by Jankovsky et al.[2]. Samples of bar geometry were

cut from a ceramic pellet using an O'Well model 3242 precision vertical diamond wire saw.
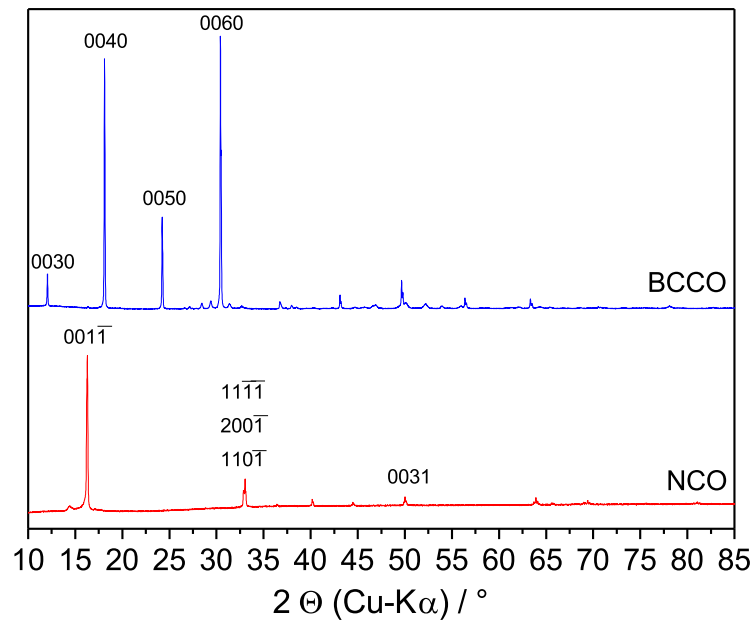
1.1 Figures

Figure S 1: XRD patterns of **NCO** and **BCCO** with indexed reflections according to superspace group C2/m^{3} and P2/m[4]. NCO and BCCO were obtained after sintering at 1073 and 1123 K for 10 hours, respectively.
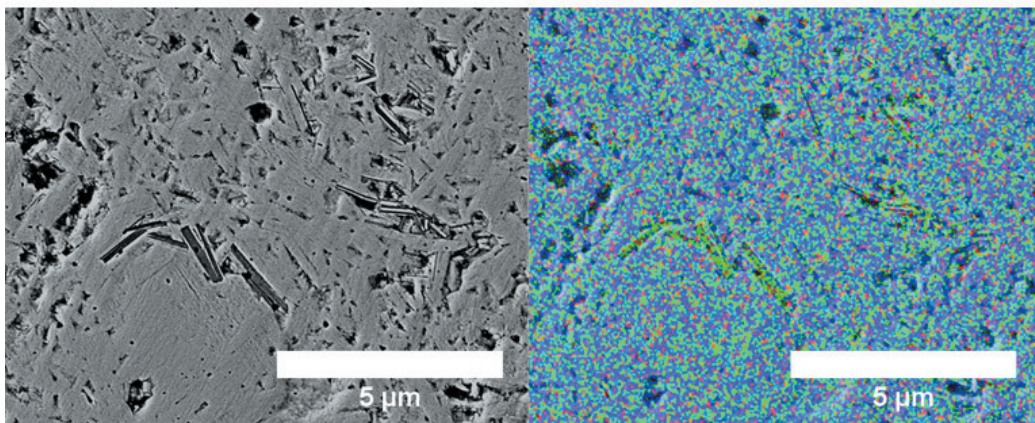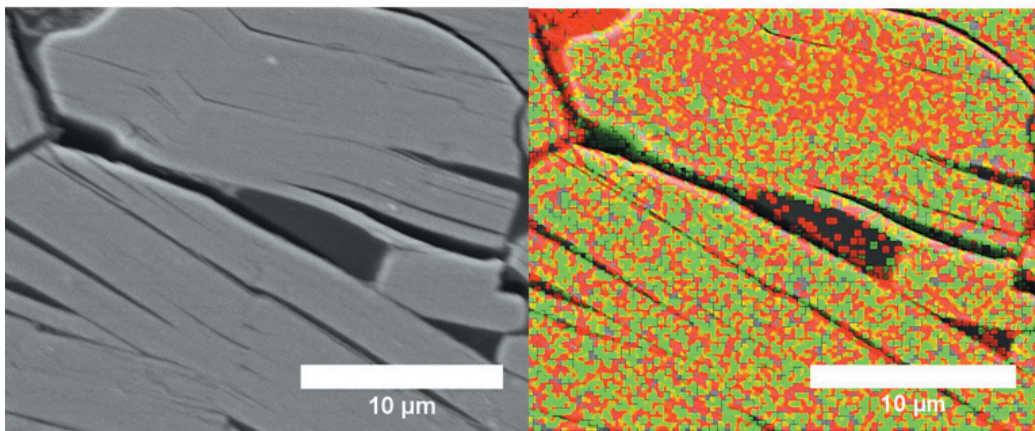
BCCO

NCO

Figure S 2: SEM cross-sectional micrographs and EDXS elemental distributions of a, b) **BCCO** ceramic (Ca-green, Bi-blue and Co-red) and c, d) **NCO** ceramic (Na-green and Co-red).
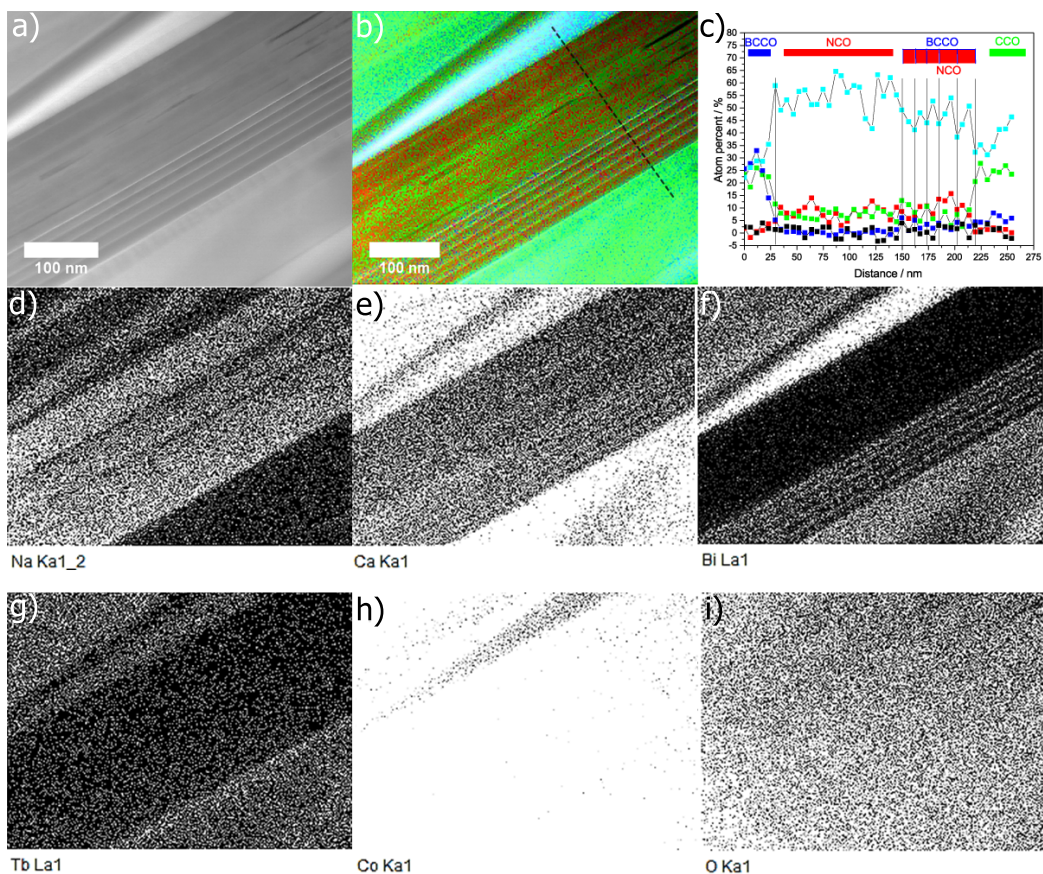
Figure S 3: TEM analysis of a **CCO-30-35-10** nanocomposite ceramic, supplementing Figure 4a-c) of the main document. a, b) STEM dark-field micrograph and EDXS elemental distribution of the region shown. c) Linescan of the elemental distribution of Na (red), Ca (green), Bi (blue), Tb (black) and Co (turquoise) shown in b). Along the indicated direction (dotted line), different phases and their compositions along the linescan are indicated. d-i) Detailed elemental distribution information for Na, Ca, Bi, Co, Tb and O.
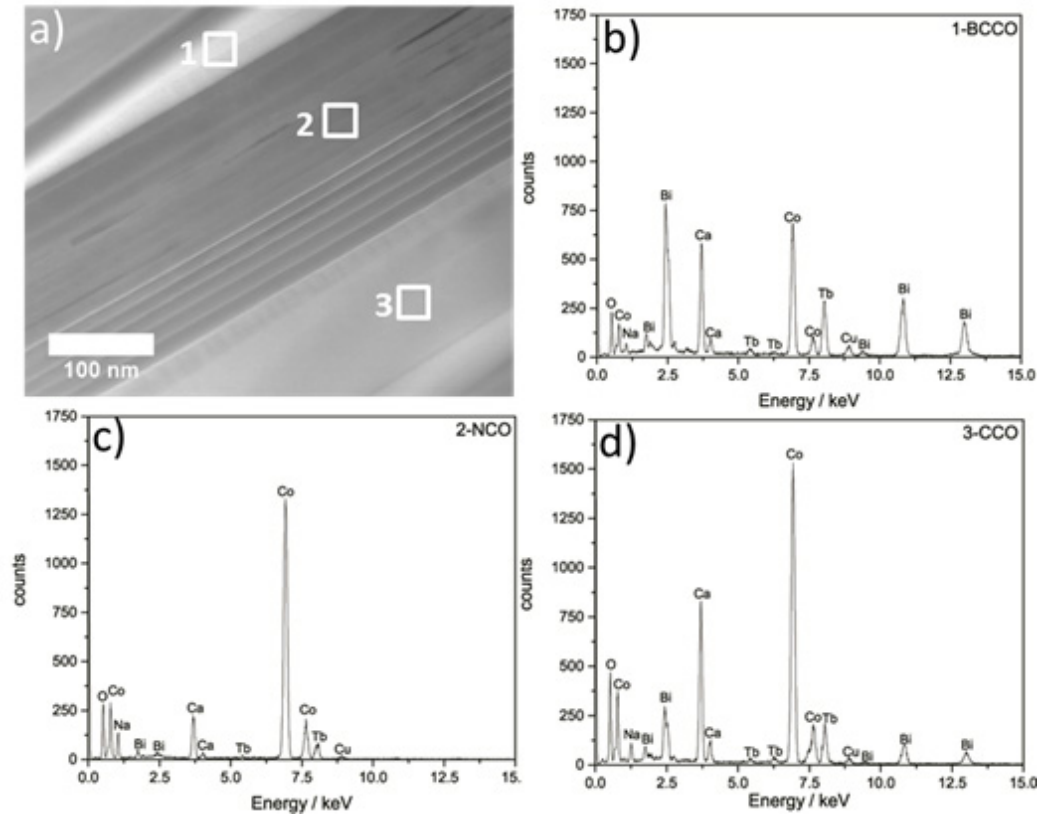
Figure S 4: TEM analysis of a **CCO-30-35-10** nanocomposite ceramic, supplementing Figure 4a-c) of the main document. a) STEM dark-field micrograph and b-d) element spectra of different phases BCCO (1), NCO (2) and CCO (3) of the regions shown.
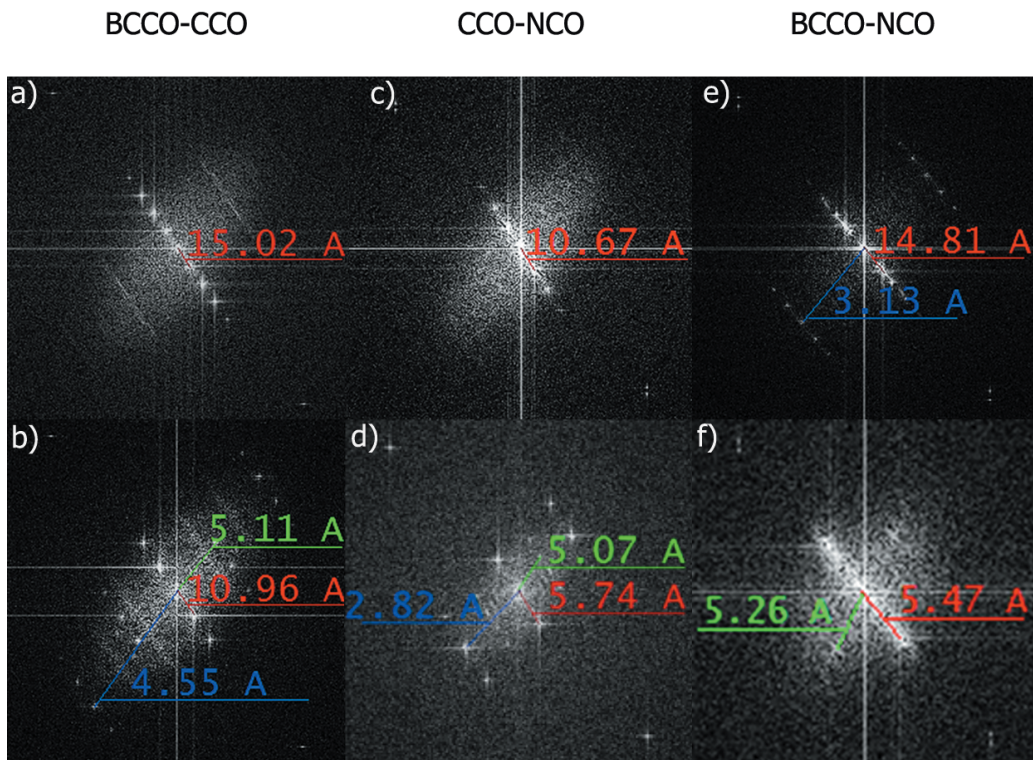
Figure S 5: Enlarged presentation of reduced fast Fourier transformations in insets of Figure 4d-f) showing the TEM analysis of a **CCO-30-35-10** nanocomposite ceramic: a, b) BCCO-CCO-interface; c, d) CCO-NCO-interface; and e, f) BCCO-NCO-interface with indicated lattice parameters of a (green), b (blue) and c (red).
BCCO-CCO: BCCO - c= 15.02 Å, CCO - a= 5.11 Å, b_2= 4.55 Å, c= 10.96 Å
CCO-NCO: CCO - c= 10.67 Å, NCO - a= 5.07 Å, b_1= 2.82 Å, c= 5.74 Å
BCCO-NCO: BCCO - b_1= 3.13 Å, c= 14.81 Å, NCO - a= 5.26 Å, c= 5.47 Å
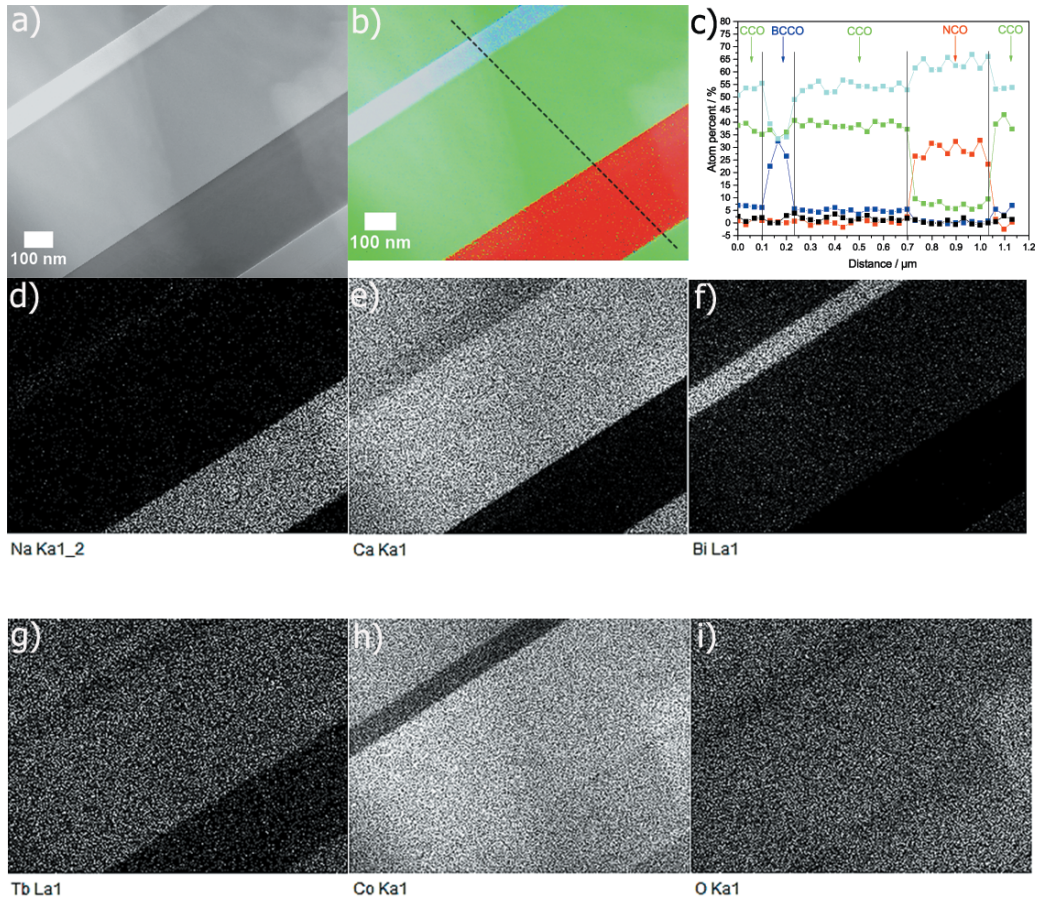
Figure S 6: TEM analysis of a second site of a **CCO-30-35-10** nanocomposite ceramic, a, b) STEM dark-field micrograph and EDXS elemental distribution of the area shown. c) Linescan of the elemental distribution of Na (red), Ca (green), Bi (blue), Tb (black) and Co (turquoise) shown in b). Along the indicated direction (dotted line), different phases and their compositions along the linescan are indicated. d-i) Detailed elemental distribution information for Na, Ca, Bi, Co, Tb and O.
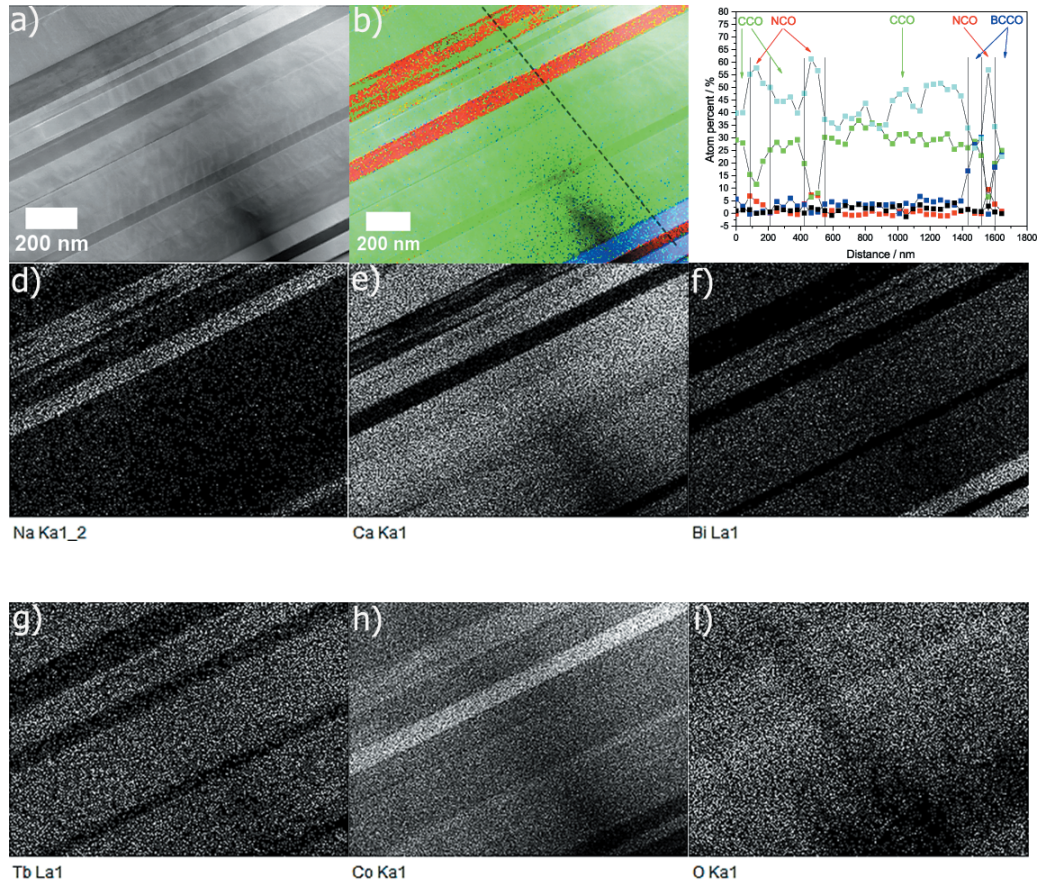
Figure S 7: TEM analysis of a third site of a **CCO-30-35-10** nanocomposite ceramic, a, b) STEM dark-field micrograph and EDXS elemental distribution of the area shown. c) Linescan of the elemental distribution of Na (red), Ca (green), Bi (blue), Tb (black) and Co (turquoise) shown in b). Along the indicated direction (dotted line), different phases and their compositions along the linescan are indicated. d-i) Detailed elemental distribution information for Na, Ca, Bi, Co, Tb and O.
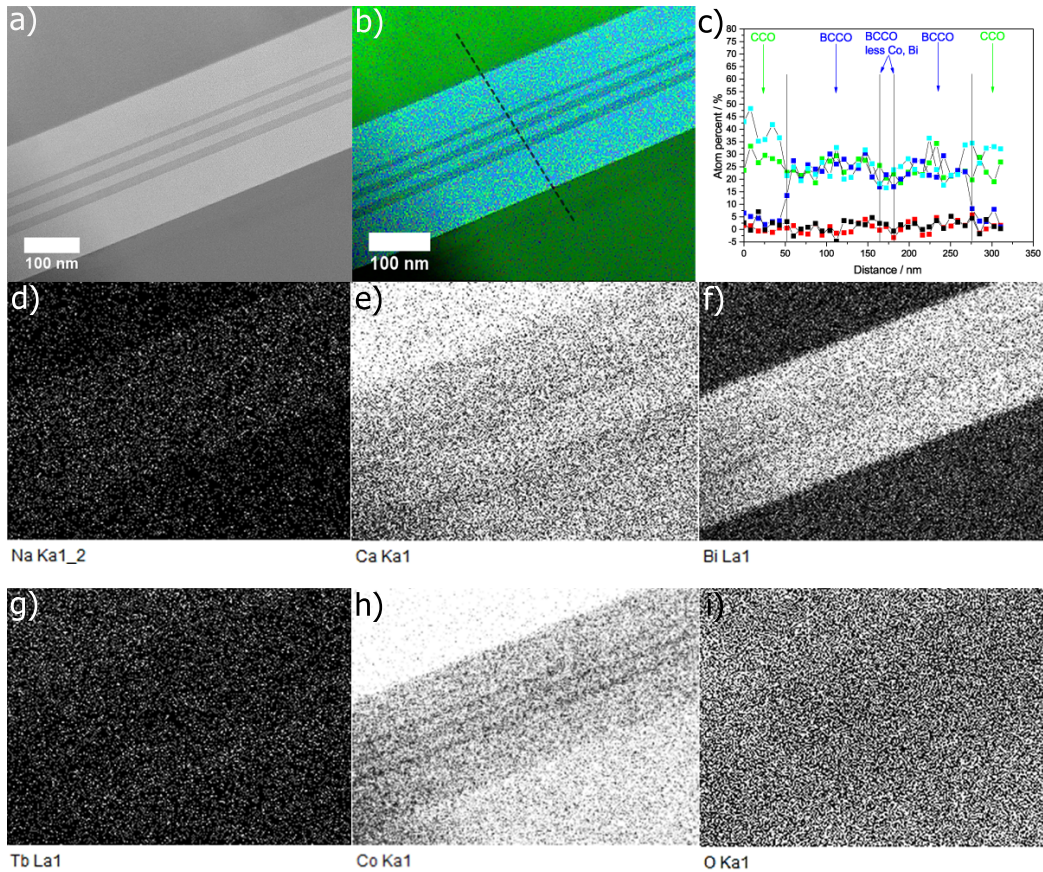
Figure S 8: TEM analysis of a fourth site of a **CCO-30-35-10** nanocomposite ceramic, a, b) STEM dark-field micrograph and EDXS elemental distribution of the area shown. c) Linescan of the elemental distribution of Na (red), Ca (green), Bi (blue), Tb (black) and Co (turquoise) shown in b). Along the indicated direction (dotted line), different phases and their compositions along the linescan are indicated. d-i) Detailed elemental distribution information for Na, Ca, Bi, Co, Tb and O.
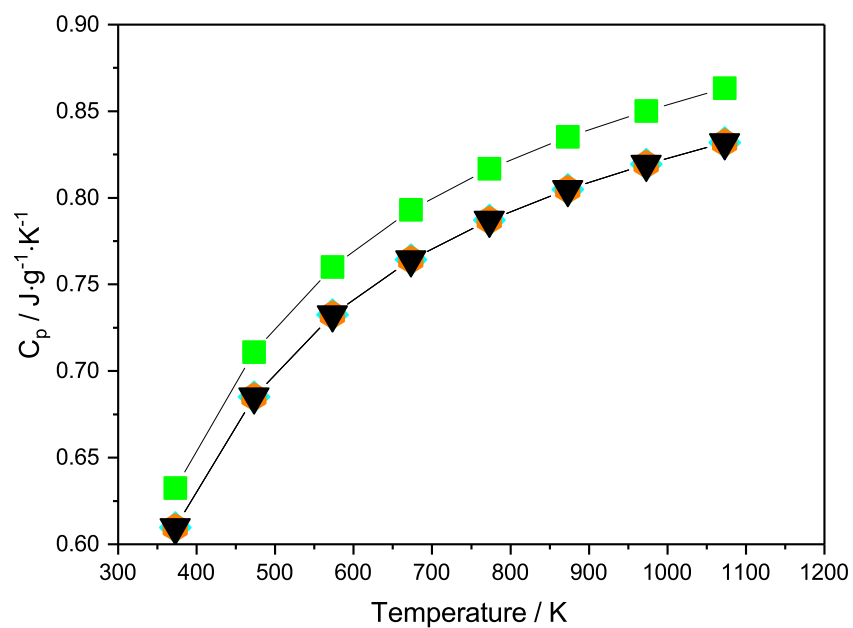
Figure S 9: Heat capacity C_P as a function of temperature of **CCO** (squares, green, taken from [5]), **CCO-30-35-6** (diamonds, turquoise), **CCO-30-35-8** (hexagons, orange) and **CCO-30-35-10** (inverted triangles, black) ceramics.

1.2 Tables

Table S 1: Ionic radii of cations and dopants in $Ca_{3-x-y-z}Na_xBi_yTb_zCo_4O_9$ [6].

Element	Ca	Na	Bi	Tb		Co	
coordination number	6	6	6	6		8	
ionic charge	+2	+1	+3	+3	+4	+3	+4
ionic radii / Å	1.12	1.18	1.17	1.04	0.88	0.61	0.53

References

[1] A. Sotelo, E. Guilmeau, S. Rasekh, M. A. Madre, S. Marinel, J. C. Diez, Enhancement of the thermoelectric properties of directionally grown Bi-Ca-Co-O through Pb for Bi substitution, J. Eur. Ceram. Soc. 30 (2010) 1815–1820.

[2] O. Jankovsky, D. Sedmidubsky, Z. Sofer, J. Hejtmanek, Thermodynamic behavior of $Ca_3Co_4O_{9+\delta}$ ceramics, Ceram-Silikaty 56(2) (2012) 139–144.

[3] L. Viciu, J. W. G. Bos, H. W. Zandbergen, Q. Huang, M. L. Foo, S. Ishiwata, A. P. Ramirez, M. Lee, N. P. Ong, R. J. Cava, Crystal structure and elementary properties of Na_xCoO_2 (x = 0.32, 0.51, 0.6, 0.75, and 0.92) in the three-layer $NaCoO_2$ family, Phys. Rev. B 73 (2006) 174104–1–174104–10.

[4] E. Guilmeau, M. Pollet, D. Grebille, M. Hervieu, M. Muguerra, R. Cloots, M. Mikami, R. Funahashi, Nanoblock coupling effect in iodine intercalated $[Bi_{0.82}CaO_2]_2[CoO_2]_{1.69}$ layered cobaltite, Inorg. Chem. 46 (2007) 2124–2131.

[5] M. Bittner, L. Helmich, F. Nietschke, B. Geppert, O. Oeckler, A. Feldhoff, Porous $Ca_3Co_4O_9$ with enhanced thermoelectric properties derived from sol-gel synthesis, J. Eur. Ceram. Soc. 37 (2017) 3909–3915.

[6] R. D. Shannon, Revised effective ionic radii and systematic studies of interatomic distances in halides and chalcogenides, Acta Cryst. A32 (1976) 751–767.